


Communication

Enhancement in Charge Carrier Mobility by Using Furan as Spacer in Thieno[3,2-b]Pyrrole and Alkylated-Diketopyrrolopyrrole Based Conjugated Copolymers

Prabhath L. Gamage, Chinthaka M. Udamulle Gedara, Ruwan Gunawardhana, Chandima Bulumulla, Ziyuan Ma, Ashutosh Shrivastava, Michael C. Biewer * and Mihaela C. Stefan * 

The Department of Chemistry and Biochemistry, The University of Texas at Dallas, Richardson, TX 75080, USA; plg150030@utdallas.edu (P.L.G.); cxu160230@utdallas.edu (C.M.U.G.); kxg141730@utdallas.edu (R.G.); bulumullac@janelia.hhmi.org (C.B.); zxm180001@utdallas.edu (Z.M.); ashutosh.shrivastava@utdallas.edu (A.S.)

* Correspondence: biewerm@utdallas.edu (M.C.B.); mihaela@utdallas.edu (M.C.S.)

Abstract: The structural alteration of semiconducting polymer backbones can improve the optoelectronic properties of organic semiconductors and enhance field-effect mobilities. In our efforts towards improving the performance of organic field-effect transistors (OFETs), we are reporting a donor–acceptor polymer containing thieno[3,2-b]pyrrole (TP) donor and a furan-flanked diketopyrrolopyrrole (DPP) electron acceptor, which yielded an asymmetric poly(methylthienopyrrolo)furanyl diketopyrrolopyrrol) **P(FDPP-TP)** organic semiconducting polymer. The introduction of a furan spacer improved thermally induced crystallinity and molecular packing, as confirmed by grazing incidence X-ray diffraction (XRD) and tapping-mode atomic force microscopy (TMAFM). The tested OFET devices gave maximum hole mobility of $0.42 \text{ cm}^2 \text{ V}^{-1} \text{ s}^{-1}$ with threshold voltages around 0 V for bottom-gate bottom-contact device configuration.

Keywords: pyrrole; diketopyrrolopyrrole; furan; organic electronics; organic semiconductors; organic field-effect transistors



Citation: Gamage, P.L.; Udamulle Gedara, C.M.; Gunawardhana, R.; Bulumulla, C.; Ma, Z.; Shrivastava, A.; Biewer, M.C.; Stefan, M.C. Enhancement in Charge Carrier Mobility by Using Furan as Spacer in Thieno[3,2-b]Pyrrole and Alkylated-Diketopyrrolopyrrole Based Conjugated Copolymers. *Appl. Sci.* **2022**, *12*, 3150. <https://doi.org/10.3390/app12063150>

Academic Editors: Catalin Zaharia and Ionut-Cristian Radu

Received: 19 February 2022

Accepted: 17 March 2022

Published: 19 March 2022

Publisher's Note: MDPI stays neutral with regard to jurisdictional claims in published maps and institutional affiliations.



Copyright: © 2022 by the authors. Licensee MDPI, Basel, Switzerland. This article is an open access article distributed under the terms and conditions of the Creative Commons Attribution (CC BY) license (<https://creativecommons.org/licenses/by/4.0/>).

1. Introduction

Organic semiconducting polymers have been extensively studied for their potential application in various electronic devices such as organic field-effect transistors, organic light-emitting diodes, photovoltaics, and sensors due to their unique properties such as light weight, large area solution processibility, varied optical bandgap, and mechanical flexibility [1–9].

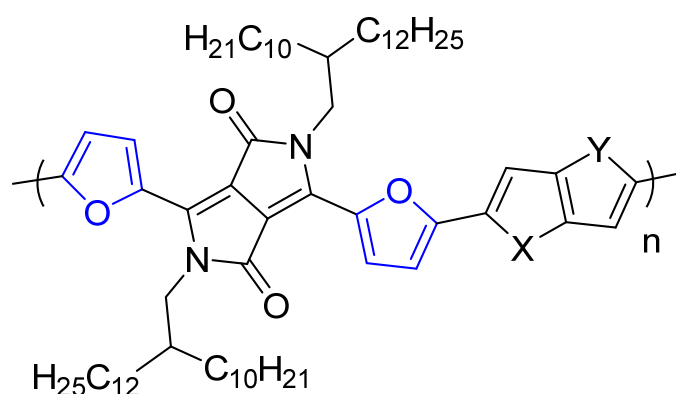
Organic field-effect transistors (OFETs) have been developed as an alternative class of FETs that could be used in bioelectronic applications. Over the last two decades, significant improvements have been achieved through advanced molecular design, side-chain engineering, and device optimization [10–14]. Organic semiconducting polymers hold the edge over the conjugated small molecules when fabricating solution-based thin films due to the relatively high viscosity gained from the relatively high conjugation lengths [15–18]. Among many factors that could be considered in developing polymeric backbones with improved intrinsic charge carrier mobility, solid-state molecular packing is essential, which has to be achieved by careful design of donor–acceptor alternating copolymers [19–23]. The donor–acceptor copolymer approach provides the advantage of mixing orbitals of donor–acceptor units, coupled alternately in π -conjugated polymer that eventually helps in tailoring the electronic bandgap of the material [24]. Out of many π -electron acceptors employed in OFETs, the diketopyrrolopyrrole (DPP) unit has been identified as one of the most efficient acceptor units due to its high unipolar ambipolar charge carrier mobilities associated with strong aggregation properties [10,22,25–27]. Apart from the π -electron acceptor, the selection of the π -electron donor is equally critical as it plays a significant

role in adjusting inter/intramolecular interactions, hence benefitting molecular packing. Symmetric donor blocks, for example, *e*, are heavily utilized as electron-rich moieties to make regio-regular semiconducting polymers [28,29]. However, in previous work reported by our group, we used the asymmetric donor, thieno[3,2-*b*]pyrrole (TP), which is an electron-rich versatile building block that also allows for an easy modification through *N*-alkylation reactions [21,26,30–36]. Even though it was estimated that the pyrrole unit would be prone to oxidation, it was demonstrated that fused TP moiety is stable enough to realize OFET applications [26,31–33].

Apart from the molecular backbone, side-chain density also plays a critical role in solution processibility and charge transport by controlling the mesoscale assembly. The orientation of the side-chain attached to the backbone controls the local packing motifs and influences the electronic coupling between neighbor chains [37,38]. Out of many modifications that could be performed to impart favorable electronic properties, donor–acceptor bridging unit improvements, i.e., spacer group improvements, tend to be more prominent as this unit changes the polymer backbone, which regulates charge transport [25,39–41]. The furan spacer group is expected to provide smaller π -packing distances and better backbone planarity due to the small atomic size of oxygen, which is advantageous for charge-carrier transportation.

Despite the main focus being on the OFET performance, one of the experimental observations that have drawn less attention is the non-linear behavior of the transfer curve observed for some high-performing organic semiconductors. Non-linear behavior often leads to an overestimation of charge carrier mobilities due to inaccurate data extraction [25,42]. As a temporary solution, researchers now report mobilities extracted from both high and low voltages; however, which mobility is valid is still a question. This situation could be circumvented if we obtain “nearly ideal” transfer curves by molecular design to better estimate OFET performances [26,43]. In the limited literature reported, TP-based OFETs have shown “nearly ideal” behavior in the transfer curves [26,32,33].

In this work, we have presented the synthesis of a new donor–acceptor-type organic semiconducting copolymer where TP and DPP were utilized as donor and acceptor, respectively (Figure 1). We used furan as donor–acceptor bridging unit, and 2-decyltetradecyl was used as a side chain to increase the solubility. We have also performed the DFT calculation to study the coplanarity of the backbone and estimate the torsional angles along the π -conjugated backbone. Finally, we have investigated this polymer’s OFETs performance, which shows maximum hole mobility of $0.42 \text{ cm}^2 \text{ V}^{-1} \text{ s}^{-1}$, which is highest among TP- and DPP-based donor–acceptor-type polymers to the best of our knowledge [31].



P(FDPP-TP); X = S, Y = N-CH₃ or X = N-CH₃, Y = S

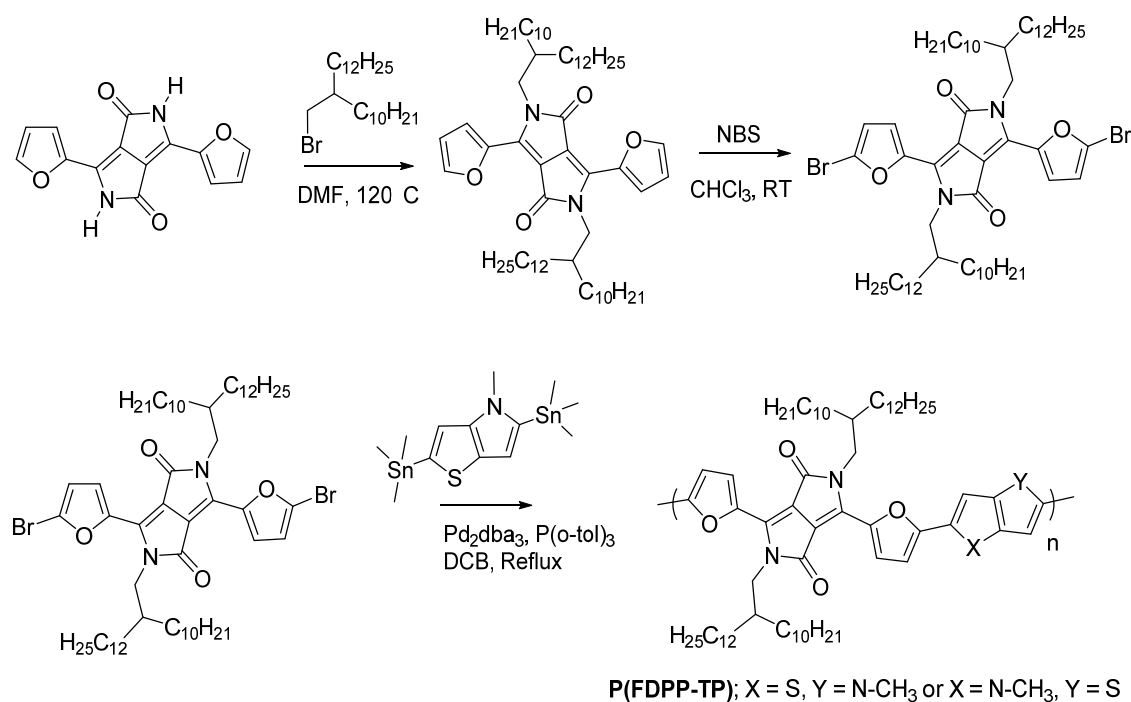
Figure 1. Structure of polymer poly(((methylthionopyrrolo)furanyl)diketopyrrolopyrrol) **P(FDPP-TP)**.

2. Experimental Section

All the experiments were performed according to previously published methods and procedures [26]. A detailed description of the experimental techniques used in this study is included in the Supplementary Information (SI).

3. Results and Discussion

The synthesis of poly(((methylthionopyrrolo)furanyl)diketopyrrolopyrrol) **P(FDPP-TP)** is shown in Scheme 1. Compounds 3,6-di(furan-2-yl)pyrrolo[3,4-*c*]pyrrole-1,4(2*H*,5*H*)-dione and 4-methyl-2,5-bis(trimethylstannyl)-4*H*-thieno[3,2-*b*]pyrrole (monomer **M2**) were synthesized according to a method reported in a literature [26]. Alkylation of 2,5-bis(2-decyltetradecyl)-3,6-di(furan-2-yl)pyrrolo[3,4-*c*]pyrrole-1,4(2*H*,5*H*)-dione carried out with 9-(bromomethyl)nonadecane followed by bromination using NBS in chloroform yielded the new monomer 3,6-bis(5-bromofuran-2-yl)-2,5-bis(2-decyltetradecyl)-2,5-dihydropyrrolo[3,4-*c*]pyrrole-1,4-dione (**M1**). The detailed synthesis of monomer **M1** is included in the Supplementary Information (SI). Polymer synthesis was carried out with the Stille coupling polymerization reaction between **M1** and **M2** in anhydrous *o*-dichlorobenzene using Pd₂(dba)₃ catalyst and P(*o*-tolyl)₃ ligand. After stirring at 130 °C for 36 h in a pressure flask under a nitrogen atmosphere, the polymerization reaction mixture was brought to room temperature and subsequently precipitated out in methanol. Successive Soxhlet extractions with methanol, acetone, and hexanes were performed for the crude solid before the final polymer product was collected into chloroform. The number average molecular weight (M_n) of the polymer **P(FDPP-TP)** was 18.6 kDa with a PDI of 1.62, estimated from size exclusion chromatography using tetrahydrofuran solvent. The detailed procedure and characterization of synthesized polymer **P(FDPP-TP)** are included in the SI (Figure S1–S5).



Scheme 1. Synthesis of poly(((methylthionopyrrolo)furanyl)diketopyrrolopyrrol) **P(FDPP-TP)**.

The optical properties of the polymer in both solutions (CHCl₃) and thin film were studied with UV-Vis spectroscopy. The UV-Vis absorption spectra obtained for **P(FDPP-TP)** are shown in Figure 2a. In solution, two peaks were observed at 395 and 832 nm, attributed to π - π^* charge transfer and donor-acceptor charge transfer, respectively.

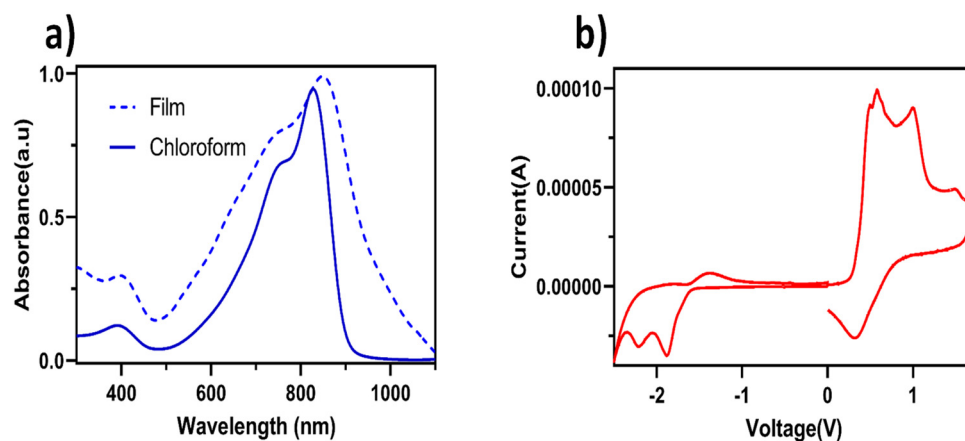


Figure 2. (a) UV-Vis spectrum; (b) Cyclic voltammogram of **P(FDPP-TP)**.

In thin film, both peaks were red-shifted to 402 and 870 nm, indicating a favorable π -stacking between solid-state polymer chains, beneficial for charge carrier transport. The optical bandgap was 1.25 eV as calculated with the onset wavelength (1040 nm) of the polymer's solid-state absorbance spectrum.

The experimental HOMO and LUMO energy levels of **P(FDPP-TP)** were determined using cyclic voltammetry (CV). The HOMO and LUMO energies were calculated using the onset potentials of oxidation and reduction peaks of the cyclic voltammogram. The equations $E_{HOMO} = -(E_{ox} + 4.4)$ eV and $E_{LUMO} = -(E_{red} + 4.4)$ eV were applied respectively to calculate HOMO and LUMO levels. The HOMO and LUMO energy levels were determined to be -4.64 eV and -2.77 eV, respectively. The HOMO energy level, close to the Au work function (-5.1 eV), is expected to facilitate the hole injection from gold contacts in the p-type polymers [25,44]. The calculated electrochemical bandgap was 1.87 eV from CV measurements. The observed disparity in the optical and electrochemical bandgaps (0.62 eV) can be attributable to the material's exciton binding energy, which could vary between 0.4 and 1.0 eV [21,22,26]. Optoelectronic properties of **P(FDPP-TP)** were summarized in Table S1.

Spartan 16 software at B3LYP/6-31G* theory level was used to estimate the coplanarity of the backbone and torsional angles to calculate the theoretical electronic energy levels of the **P(FDPP-TP)** dimer replacing alkyl substituents with the methyl groups (Figure S6). The DPP unit had a slight twist between the DPP and the flanker unit furan, while the asymmetric thieno[3,2-*b*]pyrrole unit had two different angles on either side. The furan unit made a relatively low dihedral angle of 1.92° with the thiophene side of TP as expected, giving a better coplanarity to the polymer backbone, and the calculated torsional angle between the furan and pyrrole side of TP is 11.55° . Coplanarity of the molecule is expected to have frontier orbitals delocalized through the polymer's backbone, which might be beneficial to increase charge carrier mobility.

Thermal properties of the **P(FDPP-TP)** polymer were investigated with TGA and DSC. The respective TGA curve and DSC traces are included in Figure S9. The 5% decomposition in the TGA thermogram of **P(FDPP-TP)** polymer was observed until 160°C temperature, which may be due to adsorbed solvent molecules on the surface of the polymer, whereas the onset of melting was observed at 262°C in the heating cycle of the DSC, reflecting the possible crystalline nature of the polymer.

The OFET performance of **P(FDPP-TP)** was studied with both BGBC and BGTC device architectures, and **P(FDPP-TP)** polymer showed p-type OFET characteristics. A summary of the OFET performance for BGBC devices is shown in Table S2, and the corresponding transfer and output curves are presented in Figure 3. The hole mobilities were calculated from the transfer curves obtained at different annealing temperatures. For BGBC devices, maximum hole mobility of $4.46 \times 10^{-3} \text{ cm}^2 \text{ V}^{-1} \text{ s}^{-1}$ was measured, and the on/off ratio was $\sim 10^3$, without thermal annealing treatment. After annealing at 150°C for 5 min,

the hole mobility showed a 10-fold increase compared to the value measured for non-annealed devices. Once the annealing temperature was increased to 200 °C, the maximum hole mobility had a value of $0.42 \text{ cm}^2 \text{ V}^{-1} \text{ s}^{-1}$, and the on/off ratio also increased to 10^5 . This improvement is similar to reported DPP polymers in the literature [27,39,44,45]. At low annealing temperatures, the threshold voltages varied between -2 and -7 V. The temperatures higher than 200 °C resulted in a reduction in the hole mobility, which may be due to the thermal degradation of the polymer suggested by the TGA data.

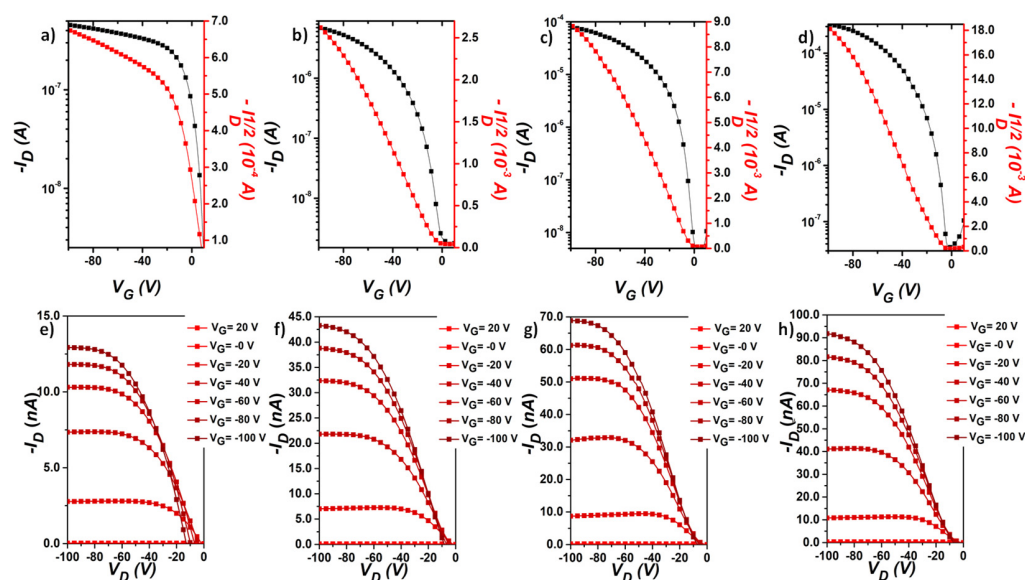


Figure 3. Bottom-gate bottom-contact (BGBC) OFET characteristics for **P(FDPP-TP)** polymer. (a) Transfer curve; (e) output curve; (b) non-annealed (room temperature) transfer curve; (f) non-annealed (room temperature) output curve; (c) transfer curve at 100 °C; (g) output curve at 150 °C; (d) transfer curve at 200 °C; (h) output curve at 200 °C.

The BGTC devices showed the same trend in the hole mobility, and the maximum mobility obtained was $0.127 \text{ cm}^2 \text{ V}^{-1} \text{ s}^{-1}$ at 200 °C. Corresponding transfer and output plots are shown in Figures S7 and S8. A summary of the OFET parameters is included in Table S3. For the BGTC devices, the maximum mobility measured was $2.62 \times 10^{-3} \text{ cm}^2 \text{ V}^{-1} \text{ s}^{-1}$ at room temperature. Upon annealing, it showed an increase of ~ 100 -fold at 200 °C, retaining the on/off ratio higher than 10^5 , indicating that intrinsic hole mobility is independent of the device architecture used. The optimized conditions for both the device architectures showed better device performance concerning hole mobility and on/off switch-ratio than our previously reported **P(DPP-TP)** polymer with the thiophene spacer group [26]. The **P(FDPP-TP)** showed four times higher maximum hole mobility compared to the maximum mobility reported for **P(DPP-TP)**, and the on/off ratio was 10^2 times higher than that of **P(DPP-TP)**.

The transfer curves of the devices showed improved “linear” behavior upon annealing. They showed two gradients at lower temperatures, but the transistors reached the nearly ideal behavior leading to “linear” plots for both BGBC and BGTC devices for the annealed films. For most of the DPP-based polymers, the mobility calculation has suffered from the non-ideal behavior of the transfer curves [25,26,31,33], and the transistor behavior of TP-based polymers has shown its ability to be utilized as a better candidate for improved OFET applications. Moreover, the spacer unit’s change from thiophene to furan in DPP copolymers with thienylenevinylene (TVT) has dramatically increased the hole mobility of furan-based DPP, a promising building block for a vast range of semiconducting polymers for organic electronics [40,41].

The grazing incidence X-ray diffraction (GIXRD) analysis was carried out on the polymer thin films deposited on SiO_2 substrates (OTMS treated) by employing the same

conditions applied for the fabrication of OFETs, to investigate crystallinity. The GIXRD out-of-plane patterns at different annealing temperatures are presented in Figure 4. Both annealed and non-annealed polymer thin films showed a diffraction peak of around 3.80° which arose from the (100) crystalline plane. However, the intensity of this peak increases gradually upon annealing to higher temperatures. Another diffraction peak can be observed around 7.25° upon annealing, which was not present in the non-annealed (RT) sample. This second Bragg reflection peak could be due to the (200) diffraction planes, which indicates the polymer's enhanced crystallinity upon annealing to higher temperatures, which is reflected in increased mobilities upon annealing. Apart from these two lamellar peaks, there is a broad peak around 21.10° in the spectra. Even though the enhancement of the peak intensity was not as dramatic as lamellar peaks, this weak diffraction indicates possible π - π stacking existing between the polymer chains that aid the carrier transport among the polymer chains. An additional (200) plane shows enhanced crystallinity which is probably due to the close polymer chain proximity from the smaller atom-size of oxygen on furan. These data indicate that greater crystallinity and more compact polymer chain packing observed from the GIXRD explain the higher hole mobility of the annealed samples, from which it can be concluded that the thermally induced crystallinity has aided in enhancing the performance of the thin-film devices. Table 1 and Figure S10 summarize the GIXRD data of the P(FDPP-TP).

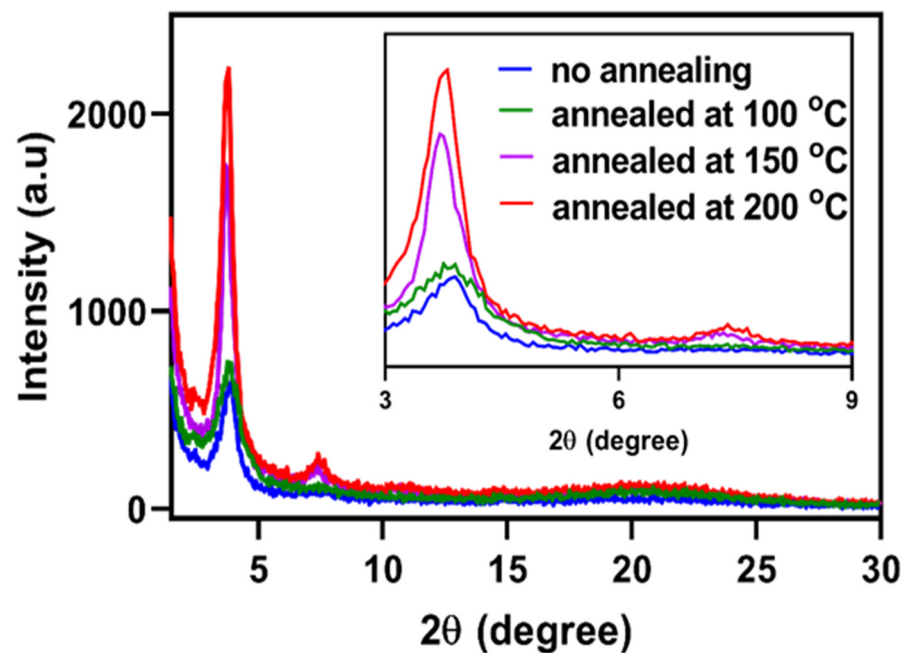


Figure 4. GIXRD pattern of annealed P(FDPP-TP) thin films at different temperatures on SiO₂ substrates treated with octadecyl trimethoxy silane (OTMS).

Table 1. GIXRD data of the P(FDPP-TP) polymer.

Peak	2θ (Deg)	D Spacing (Å°)
(100)	3.80	23.20
(200)	7.25	12.15
(010)	21.10	4.18

The channel regions of OFET devices were subjected to tapping mode atomic force microscopy (TMAFM) imaging to investigate the thin-film surface morphology. TMAFM images obtained for corresponding thin films are shown in Figure 5.

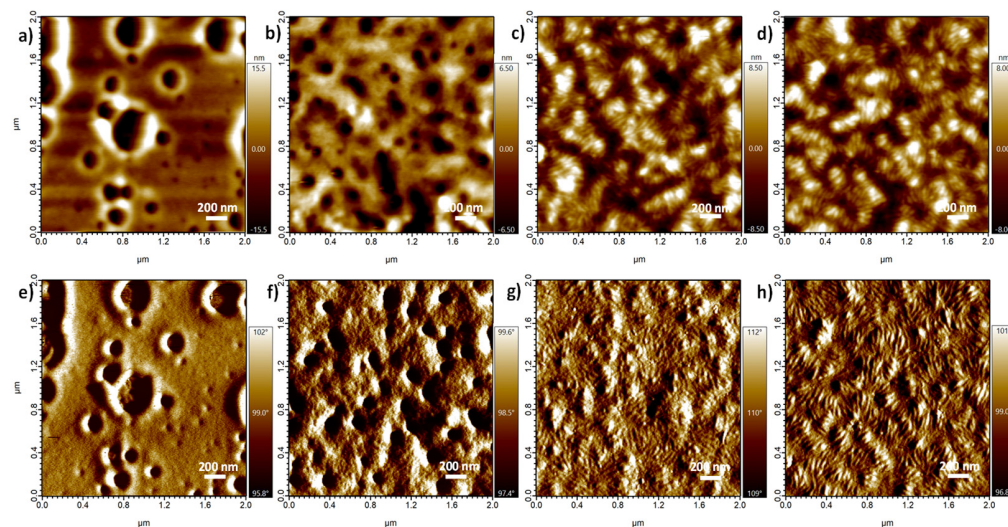


Figure 5. AFM images of **P(FDPP-TP)**: (a–d) height images; (e–h) phase images at different annealing temperatures; (a,e) non-annealed films; (b,f) annealed at 100 °C; (c,g) annealed at 150 °C; (d,h) annealed at 200 °C.

The thin films prepared at room temperature showed relatively irregular small aggregated morphology, whereas the annealing induced more ordered granular structures, as shown in the annealed film phase images.

For the films annealed at 150 °C and 200 °C, the phase images show fibril-like aggregates arranged in a more orderly pattern, indicating enhanced intermolecular packing in thin films, facilitating the charge transport in the semiconductor. The calculated root mean square values (RMS) for the annealed surfaces (3.37 nm, 3.88 nm, and 4.20 nm for 100 °C, 150 °C, and 200 °C, respectively) also suggest that the domain size has changed with these more orderly patterns, increasing the surface roughness. The same fibrillous nature in the aggregates has been observed in high-performing semiconducting polymer thin films in literature [29,46]. Hence, it was confirmed that the annealing had induced the fibrillary arrangement in the thin film of **P(FDPP-TP)**, which is beneficial in the charge carrier mechanism reflected in the better device performance.

4. Conclusions

In summary, a novel donor–acceptor copolymer **P(FDPP-TP)** consisting of thieno[3,2-*b*]pyrrole and diketopyrrolopyrrole with furan spacer units was synthesized. The **P(FDPP-TP)** polymer showed better planarity with the furan spacer, as suggested by the DFT calculations. The UV-Vis data indicate that there might be possible π -stacking and lamellar packing in the solid-state polymer. The highest hole mobility of $0.42 \text{ cm}^2 \text{ V}^{-1} \text{ s}^{-1}$ measured in the BGBC device annealed at 200 °C for **P(FDPP-TP)** was four times higher than that of **P(DPP-TP)** [26]. Moreover, the on/off ratio was 10^2 times larger than that of **P(DPP-TP)**. Furthermore, the GIXRD and AFM data confirmed that thermal annealing increased the polymer’s crystallinity and fibrillar arrangement in thin films to facilitate the improvement of charge carrier mobilities. Additionally, it is noteworthy that employing furan as a spacer unit in TP- and DPP-based donor–acceptor-type polymers could enhance OFET performances compared to thiophene spacer.

Supplementary Materials: The following supporting information can be downloaded at: <https://www.mdpi.com/article/10.3390/app12063150/s1>, Detailed experimental methods, detailed synthesis methods of materials, NMR spectra, DFT calculations, OFET transfer and output curves, and DSC and TGA spectra of **P(FDPP-TP)** are included in the Supplementary Materials. Scheme S1: Synthesis of the poly(((methylthionopyrrolo)furan-yl)diketopyrrolopyrrole) **P(FDPP-TP)** [26,47]. Figure S1: ¹HNMR spectrum of 2,5-bis(2-decyltetradecyl)-3,6-di(furan-2-yl)-2,5-dihydropyrrolo[3,4-*c*]pyrrole-1,4-dione. Figure S2: ¹³CNMR spectrum of 2,5-bis(2-decyltetradecyl)-3,6-di(furan-2-yl)-2,5-

dihydropyrrolo[3,4-c]pyrrole-1,4-dione. Figure S3: ¹H NMR spectrum of 3,6-bis(5-bromofuran-2-yl)-2,5-bis(2-decyltetradecyl)-2,5-dihydropyrrolo[3,4-c]pyrrole-1,4-dione. Figure S4: ¹³C NMR spectrum of 3,6-bis(5-bromofuran-2-yl)-2,5-bis(2-decyltetradecyl)-2,5-dihydropyrrolo[3,4-c]pyrrole-1,4-dione. Figure S5: ¹H NMR spectrum of P(FDPP-TP) polymer. Figure S6: DFT calculation data of Spartan 16 software (B3LYP/6-31G*). Figure S7: OFET transfer curves (a-d) and output curves (e-h) of bottom-gate top-contact devices: (a,e) RT, (b,f) 100 °C, (c,g) 150 °C, and (d,h) 200 °C. Figure S8: OFET transfer curves (a,b) and output curves (c,d) at 225 °C of (a,c) BGBC and (b,d) BGTC. Figure S9: (a) DSC thermogram and (b) TGA thermogram of P(FDPP-TP). Figure S10: GIXRD pattern of P(FDPP-TP) thin films on SiO₂ substrates at different temperatures. The crystallite sizes considering (100) peak from XRD patterns were calculated by using Scherrer formula as 7.44 nm, 7.53 nm, 8.91 nm, and 9.23 nm for samples not annealed, annealed at 100 °C, annealed at 150 °C, and annealed at 200 °C, respectively [47]. Table S1: Optoelectronic properties of P(FDPP-TP). Table S2: BGBC OFET data of P(FDPP-TP). Table S3: OFET data of BGTC devices of P(FDPP-TP).

Author Contributions: Synthesis, P.L.G., C.M.U.G., R.G. and C.B.; OFET measurements, P.L.G., C.M.U.G. and Z.M.; Data analysis, preparation of manuscript, P.L.G., C.M.U.G., R.G., C.B., Z.M., A.S., M.C.B. and M.C.S. All authors have read and agreed to the published version of the manuscript.

Funding: Welch Foundation (Grant AT-1740); National Science Foundation (CHE-1609880 and CHE-1566059).

Acknowledgments: We want to acknowledge the Welch Foundation (Grant AT-1740) and the National Science Foundation (CHE-1609880 and CHE-1566059) for financial support. M.C.S. also acknowledges the Eugene McDermott Foundation for the generous endowed chair support.

Conflicts of Interest: The authors declare no conflict of interest.

References

1. Bao, Z.; Locklin, J. *Organic Field-Effect Transistors*; CRC Press: Boca Raton, FL, USA, 2007. [\[CrossRef\]](#)
2. Mullen, K.; Scherf, U. *Organic Light Emitting Devices: Synthesis, Properties and Applications*; Wiley-VCH: Weinheim, Germany, 2006.
3. Sun, S.-S.; Dalton, L.R. *Introduction to Organic Electronic and Optoelectronic Materials and Devices*; CRC Press: Boca Raton, FL, USA, 2008.
4. Brabec, C.J.; Dyakonov, V.; Scherf, U. *Organic Photovoltaics: Materials, Device Physics, and Manufacturing Technologies*; Wiley-VCH: Weinheim, Germany, 2008.
5. Grimsdale, A.C.; Leok Chan, K.; Martin, R.E.; Jokisz, P.G.; Holmes, A.B. Synthesis of Light-Emitting Conjugated Polymers for Applications in Electroluminescent Devices. *Chem. Rev.* **2009**, *109*, 897–1091. [\[CrossRef\]](#)
6. Günes, S.; Neugebauer, H.; Sariciftci, N.S. Conjugated Polymer-Based Organic Solar Cells. *Chem. Rev.* **2007**, *107*, 1324–1338. [\[CrossRef\]](#)
7. Skotheim, T.A.; Reynolds, J.R. (Eds.) *Handbook of Conducting Polymers*, 3rd ed.; CRC Press: Boca Raton, FL, USA, 2007.
8. Perepichka, D.F. (Ed.) *Handbook of Thiophene Based Materials: Applications in Organic Electronics and Photonics*; John Wiley & Sons: West Sussex, UK, 2009.
9. Beaujuge, P.M.; Amb, C.M.; Reynolds, J.R. Spectral Engineering in π -Conjugated Polymers with Intramolecular Donor-Acceptor Interactions. *Acc. Chem. Res.* **2010**, *43*, 1396–1407. [\[CrossRef\]](#)
10. Muccini, M. A bright future for organic field-effect transistors. *Nat. Mater.* **2006**, *5*, 605–613. [\[CrossRef\]](#)
11. Wang, C.; Dong, H.; Hu, W.; Liu, Y.; Zhu, D. Semiconducting π -Conjugated Systems in Field-Effect Transistors: A Material Odyssey of Organic Electronics. *Chem. Rev.* **2012**, *112*, 2208–2267. [\[CrossRef\]](#)
12. Allard, S.; Forster, M.; Souharce, B.; Thiem, H.; Scherf, U. Organic Semiconductors for Solution-Processable Field-Effect Transistors (OFETs). *Angew. Chem. Int. Ed.* **2008**, *47*, 4070–4098. [\[CrossRef\]](#)
13. Zhan, Y.; Mei, Y.; Zheng, L. Materials capability and device performance in flexible electronics for the Internet of Things. *J. Mater. Chem. C* **2014**, *2*, 1220–1232. [\[CrossRef\]](#)
14. Yan, H.; Chen, Z.; Zheng, Y.; Newman, C.; Quinn, J.R.; Dötz, F.; Kastler, M.; Facchetti, A. A high-mobility electron-transporting polymer for printed transistors. *Nature* **2009**, *457*, 679–686. [\[CrossRef\]](#)
15. Arias, A.C.; MacKenzie, J.D.; McCulloch, I.; Rivnay, J.; Salleo, A. Materials and Applications for Large Area Electronics: Solution-Based Approaches. *Chem. Rev.* **2010**, *110*, 3–24. [\[CrossRef\]](#)
16. Fu, B.; Baltazar, J.; Sankar, A.R.; Chu, P.-H.; Zhang, S.; Collard, D.M.; Reichmanis, E. Enhancing Field-Effect Mobility of Conjugated Polymers Through Rational Design of Branched Side Chains. *Adv. Funct. Mater.* **2014**, *24*, 3734–3744. [\[CrossRef\]](#)
17. Imae, I.; Tada, N.; Harima, Y. Tuning of electronic properties of novel donor-acceptor polymers containing oligothiophenes with electron-withdrawing ester groups. *Polym. Bull.* **2020**, *78*, 2341–2355. [\[CrossRef\]](#)
18. Janssen, R.A.J.; Nelson, J. Factors Limiting Device Efficiency in Organic Photovoltaics. *Adv. Mater.* **2013**, *25*, 1847–1858. [\[CrossRef\]](#)

19. Lee, M.-H.; Kim, J.; Kang, M.; Kim, J.; Kang, B.; Hwang, H.; Cho, K.; Kim, D.-Y. Precise Side-Chain Engineering of Thienylenevinylene–Benzotriazole-Based Conjugated Polymers with Coplanar Backbone for Organic Field Effect Transistors and CMOS-like Inverters. *ACS Appl. Mater. Interfaces* **2017**, *9*, 2758–2766. [[CrossRef](#)]
20. Lei, T.; Cao, Y.; Zhou, X.; Peng, Y.; Bian, J.; Pei, J. Systematic Investigation of Isoindigo-Based Polymeric Field-Effect Transistors: Design Strategy and Impact of Polymer Symmetry and Backbone Curvature. *Chem. Mater.* **2012**, *24*, 1762–1770. [[CrossRef](#)]
21. Zhu, Y.; Champion, R.D.; Jenekhe, S.A. Conjugated Donor–Acceptor Copolymer Semiconductors with Large Intramolecular Charge Transfer: Synthesis, Optical Properties, Electrochemistry, and Field Effect Carrier Mobility of Thienopyrazine-Based Copolymers. *Macromolecules* **2006**, *39*, 8712–8719. [[CrossRef](#)]
22. Gur, I.; Fromer, N.A.; Geier, M.L.; Alivisatos, A.P. Air-Stable All-Inorganic Nanocrystal Solar Cells Processed from Solution. *Science* **2005**, *310*, 462–465. [[CrossRef](#)]
23. Lei, T.; Dou, J.-H.; Pei, J. Influence of Alkyl Chain Branching Positions on the Hole Mobilities of Polymer Thin-Film Transistors. *Adv. Mater.* **2012**, *24*, 6457–6461. [[CrossRef](#)]
24. Frank, A.; Arroyave, F.A.; Richard, C.A.; Reynolds, J.R. Efficient Synthesis of Benzo[1,2-b:6,5-b⁰]dithiophene-4,5-dione (BDTD) and Its Chemical Transformations into Precursors for π -Conjugated Materials. *Org. Lett.* **2012**, *14*, 6138–6141.
25. Du, J.; Bulumulla, C.; Mejia, I.; McCandless, G.T.; Biewer, M.C.; Stefan, M.C. Evaluation of (E)-1,2-di(furan-2-yl)ethene as building unit in diketopyrrolopyrrole alternating copolymers for transistors. *Polym. Chem.* **2017**, *8*, 6181–6187. [[CrossRef](#)]
26. Bulumulla, C.; Kularatne, R.N.; Gunawardhana, R.; Nguyen, H.Q.; McCandless, G.T.; Biewer, M.C.; Stefan, M.C. Incorporation of Thieno[3,2-b]pyrrole into Diketopyrrolopyrrole-Based Copolymers for Efficient Organic Field Effect Transistors. *ACS Macro Lett.* **2018**, *7*, 629–634. [[CrossRef](#)]
27. Ha, T.-J.; Sonar, P.; Dodabalapur, A. Improved Performance in Diketopyrrolopyrrole-Based Transistors with Bilayer Gate Dielectrics. *ACS Appl. Mater. Interfaces* **2014**, *6*, 3170–3175. [[CrossRef](#)]
28. Heeney, M.; Bailey, C.; Genevicius, K.; Shkunov, M.; Sparrowe, D.; Tierney, S.; McCulloch, I. Stable Polythiophene Semiconductors Incorporating Thieno[2,3-b]thiophene. *J. Am. Chem. Soc.* **2005**, *127*, 1078–1079. [[CrossRef](#)] [[PubMed](#)]
29. McCulloch, I.; Heeney, M.; Bailey, C.; Genevicius, K.; MacDonald, I.; Shkunov, M.; Sparrowe, D.; Tierney, S.; Wagner, R.; Zhang, W.; et al. Liquid-crystalline semiconducting polymers with high charge-carrier mobility. *Nat. Mater.* **2006**, *5*, 328–333. [[CrossRef](#)] [[PubMed](#)]
30. Du, J.; Fortney, A.; Washington, K.E.; Bulumulla, C.; Huang, P.; Dissanayake, D.; Biewer, M.C.; Kowalewski, T.; Stefan, M.C. Systematic Investigation of Benzodithiophene-Benzothiadiazole Isomers for Organic Photovoltaics. *ACS Appl. Mater. Interfaces* **2016**, *8*, 33025–33033. [[CrossRef](#)]
31. Bulumulla, C.; Gunawardhana, R.; Gamage, P.L.; Miller, J.T.; Kularatne, R.N.; Biewer, M.C.; Stefan, M.C. Pyrrole-Containing Semiconducting Materials: Synthesis and Applications in Organic Photovoltaics and Organic Field-Effect Transistors. *ACS Appl. Mater. Interfaces* **2020**, *12*, 32209–32232. [[CrossRef](#)] [[PubMed](#)]
32. Bulumulla, C.; Gunawardhana, R.; Kularatne, R.N.; Hill, M.E.; McCandless, G.T.; Biewer, M.C.; Stefan, M.C. Thieno[3,2-b]pyrrole-benzothiadiazole Banana-Shaped Small Molecules for Organic Field-Effect Transistors. *ACS Appl. Mater. Interfaces* **2018**, *10*, 11818–11825. [[CrossRef](#)]
33. Bulumulla, C.; Gunawardhana, R.; Yoo, S.H.; Mills, C.R.; Kularatne, R.N.; Jackson, T.N.; Biewer, M.C.; Gomez, E.D.; Stefan, M.C. The effect of single atom replacement on organic thin film transistors: Case of thieno[3,2-b]pyrrole vs. furo[3,2-b]pyrrole. *J. Mater. Chem. C* **2018**, *6*, 10050–10058. [[CrossRef](#)]
34. Gunawardhana, R.; Bulumulla, C.; Gamage, P.L.; Timmerman, A.J.; Udamulle, C.M.; Biewer, M.C.; Stefan, M.C. Thieno[3,2-b]pyrrole and Benzo[c][1,2,5]thiadiazole Donor–Acceptor Semiconductors for Organic Field-Effect Transistors. *ACS Omega* **2019**, *4*, 19676–19682. [[CrossRef](#)]
35. Bulumulla, C.; Gunawardhana, R.; Gamage, P.L.; Kularatne, R.N.; Biewer, M.C.; Stefan, M.C. π -Spacer-Linked Bisthienopyrroles with Tunable Optical Properties. *Synlett* **2018**, *29*, 2567–2571.
36. Nguyen, H.Q.; Rainbolt, E.A.; Sista, P.; Stefan, M.C. Synthesis and Polymerization of Fused-Ring Thienodipyrrole Monomers. *Macromol. Chem. Phys.* **2012**, *213*, 425–430. [[CrossRef](#)]
37. Gao, D.; Tian, K.; Zhang, W.; Huang, J.; Chen, Z.; Mao, Z.; Yu, G. Approaching high charge carrier mobility by alkylating both donor and acceptor units at the optimized position in conjugated polymers. *Polym. Chem.* **2016**, *7*, 4046–4053. [[CrossRef](#)]
38. Chen, Z.; Huang, J.; Gao, D.; Yang, J.; Zhang, W.; Ju, H.; Yu, G. Highly-soluble multi-alkylated polymer semiconductors and applications in high-performance field-effect transistors. *J. Mater. Chem. C* **2019**, *7*, 9591–9598. [[CrossRef](#)]
39. Kang, I.; An, T.K.; Hong, J.-A.; Yun, H.-J.; Kim, R.; Chung, D.S.; Park, C.E.; Kim, Y.-H.; Kwon, S.-K. Effect of Selenophene in a DPP Copolymer Incorporating a Vinyl Group for High-Performance Organic Field-Effect Transistors. *Adv. Mater.* **2013**, *25*, 524–528. [[CrossRef](#)] [[PubMed](#)]
40. Sonar, P.; Zhuo, J.-M.; Zhao, L.-H.; Lim, K.-M.; Chen, J.; Rondinone, A.J.; Singh, S.P.; Chua, L.-L.; Ho, P.K.H.; Dodabalapur, A. Furan substituted diketopyrrolopyrrole and thienylenevinylene based low bandgap copolymer for high mobility organic thin film transistors. *J. Mater. Chem.* **2012**, *22*, 17284–17292. [[CrossRef](#)]
41. Sonar, P.; Foong, T.R.B.; Singh, S.P.; Li, Y.; Dodabalapur, A. A furan-containing conjugated polymer for high mobility ambipolar organic thin film transistors. *Chem. Commun.* **2012**, *48*, 8383–8385. [[CrossRef](#)]
42. McCulloch, I.; Salleo, A.; Chabynyc, M. Avoid the kinks when measuring mobility. *Science* **2016**, *352*, 1521. [[CrossRef](#)]

43. Bittle, E.G.; Basham, J.I.; Jackson, T.N.; Jurchescu, O.D.; Gundlach, D.J. Mobility overestimation due to gated contacts in organic field-effect transistors. *Nat. Commun.* **2016**, *7*, 10908. [[CrossRef](#)] [[PubMed](#)]
44. Chen, H.; Guo, Y.; Yu, G.; Zhao, Y.; Zhang, J.; Gao, D.; Liu, H.; Liu, Y. Highly π -extended copolymers with diketopyrrolopyrrole moieties for high-performance field-effect transistors. *Adv. Mater.* **2012**, *24*, 4618–4622. [[CrossRef](#)]
45. Kang, I.; Yun, H.-J.; Chung, D.S.; Kwon, S.-K.; Kim, Y.-H. Record High Hole Mobility in Polymer Semiconductors via Side-Chain Engineering. *J. Am. Chem. Soc.* **2013**, *135*, 14896–14899. [[CrossRef](#)]
46. Kline, R.J.; McGehee, M.D. Morphology and Charge Transport in Conjugated Polymers. *J. Macromol. Sci. Part C* **2006**, *46*, 27–45. [[CrossRef](#)]
47. Patterson, A.L. The Scherrer formula for X-ray particle size determination. *Phys. Rev.* **1939**, *56*, 978–982. [[CrossRef](#)]